Water resources and flooding risk in Kumamoto based on observed hydrologic data analysis

Makoto Higashino and Heinz G. Stefan

ABSTRACT

Variability and change of precipitation were investigated in Kumamoto on Kyushu Island in southwestern Japan, to assess water resources and flooding risk. Annual precipitation, annual maximum daily precipitation, and annual maximum hourly precipitation have increased over the period from 1891 to 2018 (128 years). Trends are 26.2 mm per decade, 6.07 mm/day per decade, and 2.17 mm/h/decade, respectively. Precipitation in the rainy season (June and July) is on average 37% (ranging from 12 to 59%) of annual precipitation for the 128-year period. Maximum daily precipitation in a year occurred at Kumamoto in the rainy season in 92/128 (72%) of the years of observation from 1891 to 2018, in the typhoon (August to November) season in 23/128 (18%), and in the March to May season in 12/128 (10%). This indicates that the rainy monsoon season poses the largest daily flooding risk. A wavelet analysis revealed that from 1891 to 2018 annual precipitation and daily maximum precipitation fluctuate with 2 and 4 years periods, which may be related to the El Nino-Southern Oscillation (ENSO). It is likely that air temperature rises, ENSO and topographical characteristics contributed to an increase in precipitation in the period. The analysis also showed that typhoons hitting or approaching Kumamoto have significantly affected annual precipitation and annual maximum daily precipitation, while the interval between typhoons affecting Kumamoto has been getting longer since the 1970s.

Key words | annual precipitation, ENSO, Kumamoto, maximum daily precipitation, typhoon, water resources

Makoto Higashino (corresponding author)
Department of Civil Engineering,
National Institute of Technology, Oita College,
1666 Maki, Oita 870-0152,
Japan
E-mail: higasino@oita-ct.ac.jp

Heinz G. Stefan
Department of Civil, Environmental and Geo-
Engineering and St. Anthony Falls Laboratory,
University of Minnesota,
Minneapolis, MN 55414,
USA

HIGHLIGHTS

- Annual precipitation, annual maximum daily precipitation, and annual maximum hourly precipitation in Kumamoto, on Kyushu Island in southwest Japan, have increased from 1891 to 2018 (128 years). Trends are 26.2 mm per decade, 6.07 mm/day per decade, and 2.17 mm/h/decade, respectively. All three trends are statistically significant at the 1% level.
- Precipitation in the rainy season (June and July) is on average 37% (ranging from 12 to 59%) of annual precipitation over the period from 1891 to 2018. The correlation between rainy season precipitation and annual precipitation is strong ($R^2 = 0.66$, Figure 3).
- Maximum daily precipitation in a year occurred at Kumamoto in the wet monsoon (June and July) season in 92/128 (72%) of the years of observation from 1889 to 2018, in the typhoon (Aug to Nov) season in 23/128 (18%) of the years of observation, and in the March to May season in 12/128 (10%) of the years of observation. This is also shown in Figure 5 and indicates that the rainy monsoon season poses the largest daily flooding risk.

- A wavelet analysis revealed that precipitation in Kumamoto fluctuated from 1891 to 2018 with 2–4 years as periods, which may indicate a relationship to ENSO. It is likely that ENSO plays an important role in annual precipitation in the periods of 1890–1900, 1920–1930, 1950–1960, 1970s, and 1990–2010, because annual precipitation in a given year becomes necessarily higher or lower in phase with the ENSO.
- The analysis also showed that typhoons hitting or approaching Kumamoto have significantly contributed to annual precipitation and annual maximum daily precipitation, while the interval between typhoons affecting Kumamoto has been getting slightly longer since the 1970s.

INTRODUCTION

Hydrologic data such as annual precipitation, annual maximum daily precipitation and others are required to plan urban drainage in Japanese cities. Annual precipitation needs to be taken into account in projects of water supply and irrigation systems. Annual maximum daily precipitation is an important parameter for flooding risk management in Japan, because most Japanese rivers are short and steep, and therefore, have flashy flow regimes, especially in the monsoon season and during typhoons.

The statistics of river flows in Japan were previously considered to be stochastic and stationary in time, and public work projects of water resources and flood control were based on probability density functions of precipitation and associated flood discharges (see e.g. Chow et al. 1988; Dingman 2002). However, annual precipitation, maximum daily precipitation, and other hydrologic parameters are changing in response to global climate change (IPCC 2014).

According to the IPCC (2014), global warming caused by enhanced greenhouse effects in the atmosphere will have significant impacts on the hydrological cycle. Therefore, changes in mean stream discharges and maximum annual floods have received much attention (see e.g. Vorosmarty et al. 2000; Alcamo et al. 2003; Milly et al. 2005; Schroter et al. 2005). Effects of climate change on future precipitation and river discharges have been simulated by general circulation models (GCMs) of the Earth's atmosphere or regional climate models coupled with hydrologic models under various climate scenarios (see e.g. Palmer et al. 2008; Chen et al. 2011; Xu et al. 2013; Zhang et al. 2014; Devkota & Gyawali 2015; Tofiq & Guven 2015; Lu et al. 2016; Amin et al. 2017; Reshmidevi et al. 2017).

Simulated climate change and associated future river discharges in East Asia including the Kumamoto study region in Japan suggest either an increase in precipitation and runoff (Arnell 1999; Nohara et al. 2006) or a decrease in mean annual flow and annual flood discharges (Arora & Boer 2001). In Japan, future river discharges were predicted to rise due to increases in precipitation (Sato et al. 2012; Shrestha et al. 2016; Taniguchi 2016).

Projected changes in precipitation and river discharge may be different depending on the scenarios assumed for the simulations and resolution of the model. In addition to simulations, it is therefore advisable to analyze available climate data for the projection of precipitation and river discharges of the future. Higashino & Stefan (2019) studied the flood discharge in the Banjo River, Saiki in Kyushu, and found that annual maximum flood discharge becomes substantially higher in phase with the El Nino-Southern Oscillation (ENSO) in the Pacific for the period from 1960 to 2015. Similarly, connections between the temperature or precipitation in the Black Sea and global atmospheric indices, i.e. the North Sea Caspian Pattern, the Southern Oscillation Index, or the North Atlantic Oscillation, were investigated using wavelet analysis (Partal & Sezen 2019).

The following study focuses on Kumamoto on Kyushu Island in the southwest of Japan. The climate in Kumamoto is characterized by strong winds and typhoons. Kumamoto city has experienced flood disasters caused by very heavy rains in 1948, 1980, 1990, and 2012. Yet the water supply for the city and for irrigation comes from groundwater. The city is considering relying on surface water if groundwater becomes depleted or polluted. For flooding risk and

water resources assessments, it is necessary to understand by how much annual precipitation, daily maximum precipitation, and other hydrologic parameters will vary in response to climate change in the future.

The purpose of this study is to investigate variability and change of precipitation for annual, daily, and hourly time-scales. Observations and data collected in Kumamoto for the period from 1891 to 2018 by the Japan Meteorological Agency (JMA) were available for analysis to specify what needs to be done for flood risk and water resource management in Kumamoto in the future.

STUDY SITE AND AVAILABLE DATA

The site of this study is the city of Kumamoto on Kyushu Island, illustrated in Figure 1. Kumamoto city at 32.8°N latitude has a population of about 740,000 (2018), and is located approximately 40 km from Mt. Aso, an active volcano which reaches an elevation of 1,592 m above sea level. In Figure 1 the city of Kumamoto is roughly indicated by a circle and the location of the JMA Kumamoto weather station is shown by a square near the coast. The Shira River (74 km long), the Kikuchi River (71 km long), and the Midori River (74 km long) flow through the central district of the city which is in the Kikuka basin created by volcanic activities. These rivers are short and steep, which is typical for many rivers in Japan, and exhibit flashy flow regimes. The residence time of the surface water runoff in these rivers is on the order of 0.5–1 days. The surface area of Kumamoto city is approximately 390 km^2. Land use in the city is mixed; about 22% of the city area is urban, 42% is agricultural (mainly rice paddies), and 36% is a natural mountain region covered by forests.
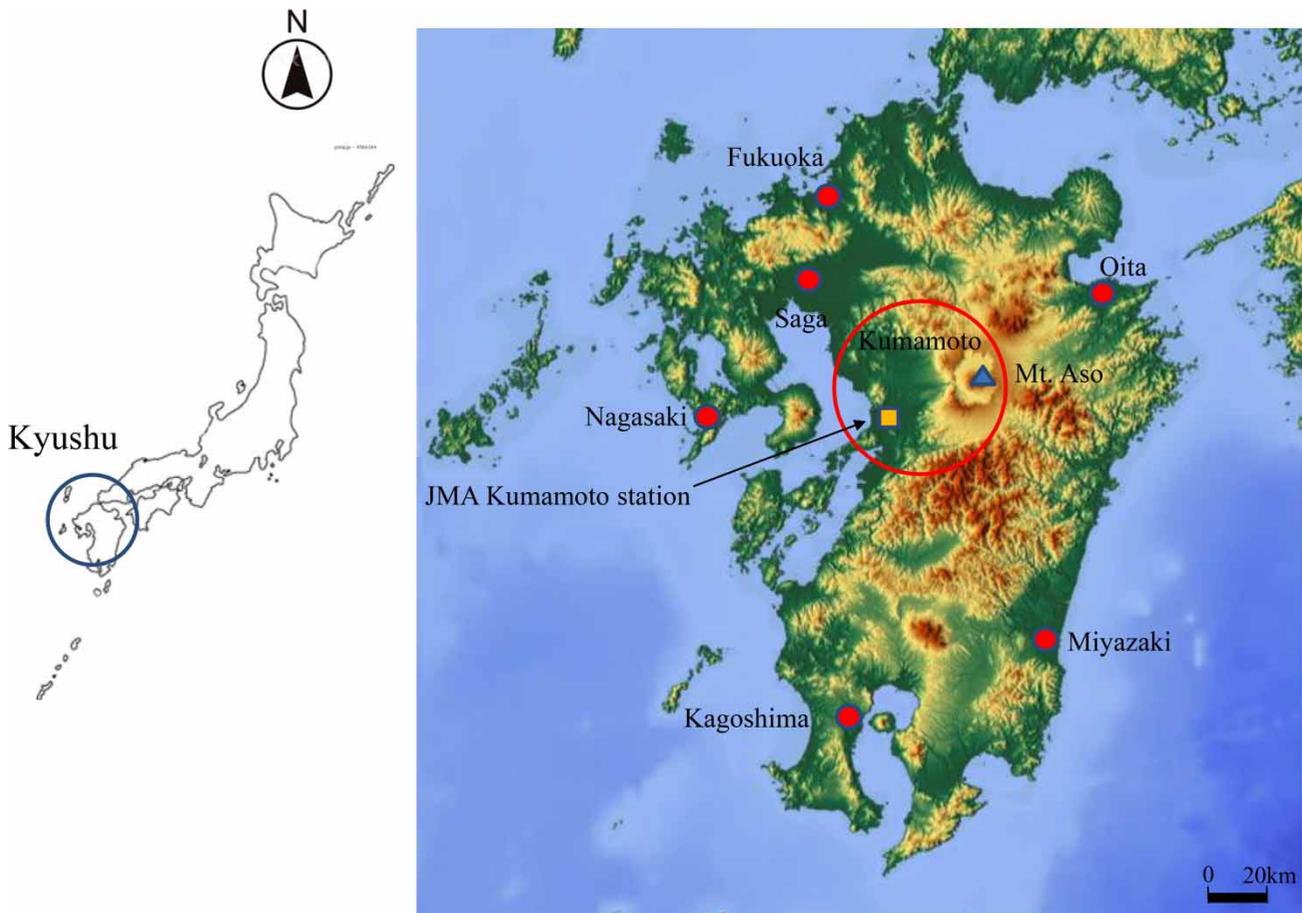
Figure 1 | Location of Kumamoto city on Kyushu Island in the southwest of Japan.

The JMA records weather data, such as air temperature and precipitation, at many locations in Japan, and data are readily available. Annual precipitation in Kumamoto from 1891 to 2018 ranged from 861.7 mm in 1894 to 3,369 mm in 1993. The average for the 128-year period was 1,892 mm, and the standard deviation was 407 mm. Precipitation is mainly due to rainfall during the rainy season (June and July) and typhoons. Precipitation during the rainy season in June and July, in addition to rainfall induced by monsoon in summer and early autumn (from June to September), ranged from 30% (1967) to 76% (2011) of annual precipitation with an average of 55% for the period. The coefficient of determination between annual precipitation and precipitation from June to September is $R^2 = 0.85$. This indicates that rainfall during the rainy and monsoon seasons contributes a large portion of the annual precipitation.

There are a few gauging stations including Kumamoto in the whole catchment shown in Figure 1. Records of precipitation at these stations are needed in order to analyze the trend in rainfall in the catchment. However, data of annual precipitation, maximum daily (24 h) precipitation, and maximum hourly precipitation are readily available at only Kumamoto station for the long term (more than a century), i.e. the 128-year period (1891–2018). Thus, this study considers that rainfall data at Kumamoto station can be representative of the catchment although it may be an over-estimation. Weather data recorded at Fukuoka, Saga, Oita, Nagasaki, Miyazaki, and Kagoshima stations were also used for comparison. The location of these sites is given in Figure 1. As summarized in Table 1, these stations are in plains, whereas only Kumamoto station is in the basin.

Table 1 | Study sites

No.	Site	Latitude	Longitude	Site class
1	Kumamoto	32.81	130.71	Basin
2	Fukuoka	33.58	130.38	Plain
3	Saga	33.27	130.31	Plain
4	Oita	33.24	131.62	Plain
5	Nagasaki	32.73	129.87	Plain
6	Miyazaki	31.94	131.41	Plain
7	Kagoshima	31.56	130.55	Plain

METHODOLOGY

Observed data of annual average air temperature, annual precipitation, annual maximum daily precipitation, and annual maximum hourly precipitation at each station from 1891 to 2018 (128 years) were obtained from the JMA website (http://www.jma.go.jp/jma/index.html) and were analyzed.

Trends over the period (1891–2018) were determined by linear regressions and are summarized in Table 2 for annual average air temperature, Table 3 for annual precipitation, Table 4 for annual maximum daily precipitation, and Table 5 for annual maximum hourly precipitation. Observed data of annual maximum hourly precipitation are available from 1891 to 2018 at only Kumamoto station. The availability of data is different at each station as shown in Table 5. The significance of trends in the data was examined by the Mann–Kendall test. Both 'Z_{MK}' and 'p' values were calculated to characterize trends and statistical significance.

Table 2 | Annual air temperature (1891–2018)

No.	Site	Trend (°C/decade)	Z_{MK}	p-value
1	Kumamoto	0.164	9.62	<0.01
2	Fukuoka	0.242	11.9	<0.01
3	Saga	0.139	9.12	<0.01
4	Oita	0.160	8.88	<0.01
5	Nagasaki	0.181	9.98	<0.01
6	Miyazaki	0.109	7.96	<0.01
7	Kagoshima	0.200	10.4	<0.01

Table 3 | Annual precipitation (1891–2018)

No.	Site	Trend (mm/decade)	Z_{MK}	p-value
1	Kumamoto	26.2	2.81	<0.01
Wet season (June–September)		25.3	2.99	<0.01
Dry season (October–May)		0.907	0.593	0.553
2	Fukuoka	9.41	1.09	0.275
3	Saga	17.5	2.30	0.0215
4	Oita	10.8	0.935	0.350
5	Nagasaki	−0.649	0.117	0.907
6	Miyazaki	7.14	0.470	0.639
7	Kagoshima	21.4	1.66	0.0969

Table 4 | Annual maximum daily precipitation (1891–2018)

No.	Site	Trend (mm/day/decade)	Z_{MK}	p-value
1	Kumamoto	6.07	4.08	<0.01
2	Fukuoka	1.63	1.92	0.0552
3	Saga	2.24	1.67	0.0956
4	Oita	1.24	0.927	0.354
5	Nagasaki	1.19	0.873	0.382
6	Miyazaki	0.688	0.521	0.602
7	Kagoshima	2.37	2.22	0.0261

Table 5 | Annual maximum hourly precipitation

No.	Site	Trend (mm/h/decade)	Z_{MK}	p-value	Data period
1	Kumamoto	2.17	5.89	<0.01	1891–2018
2	Fukuoka	1.27	3.68	<0.01	1896–2018
3	Saga	0.905	1.72	0.0856	1936–2018
4	Oita	0.941	1.33	0.182	1937–2018
5	Nagasaki	1.13	2.59	<0.01	1897–2018
6	Miyazaki	0.569	1.23	0.218	1925–2018
7	Kagoshima	1.11	2.79	<0.01	1910–2018

'Z_{MK}' given by Equation (1) is the standardized Mann–Kendall statistic which follows the standard normal distribution with a mean of 0 and a variance of 1, and 'p' is the probability value of the Mann–Kendall statistic describing the statistical significance (%).

$$Z_{MK} = \frac{S - \mathrm{sgn}(S)}{\sqrt{N(N-1)(2N+5)/18}} \qquad (1)$$

in which N is the sample size. In Equation (1), the statistic S expresses the difference between the number of concordant pairs and the number of discordant pairs, calculated using the sign function sgn(.) as:

$$S = \sum_{i=1}^{N-1} \sum_{j=i+1}^{N} \mathrm{sgn}(X_j - X_i) \qquad (2)$$

To identify the periodic components in annual precipitation, and annual maximum daily and hourly precipitation in Kumamoto from 1891 to 2018, the Daubechies 6 tap wavelet (Daubechies 1992) was used. Wavelet

transforms can be in the form of time–frequency representation for time series and have been used to investigate monthly precipitation in Matsuyama, Japan (Santos *et al.* 2001), monthly precipitation in southeast Tunisia (Jemai *et al.* 2017), annual precipitation in Bangladesh (Rahman *et al.* 2018), precipitation fluctuation in Iran (Roushangar *et al.* 2018), and rainfall time series in the mountainous basin of Urmia Lake (Farboudfam *et al.* 2018), and to capture the peak value of rainfall (Farajzadeh & Alizadeh 2017). The multiresolution-based discrete wavelet transforms of the time series $x(t)$ can be expressed as follows:

$$d_k^{(j)} = 2^j \int_{-\infty}^{\infty} \overline{\Psi(2^j x - k)} x(t) dt \qquad (3)$$

in which $d_k^{(j)}$ is the wavelet coefficient and Ψ is the wavelet function. The decomposition of the time series for the 128-year period obtained by Equation (3) is shown in Figures 9–11 for annual precipitation, maximum daily precipitation, and maximum hourly precipitation. In Equations (3) and (4), j denotes the level, i.e. levels 1, 2, 3, and 4 describe the components whose periods are 2, 4, 8, and 16 years. The time series $x(t)$ can also be reconstructed from the wavelet coefficients $d_k^{(j)}$ by the equation.

$$x(t) \sim \sum_j \sum_k d_k^{(j)} \Psi(2^j - k) \qquad (4)$$

RESULTS

Statistical analysis

As summarized in Table 2, calculated trends in annual average air temperature, over 128 years (1891–2018) at each station ranged from 0.109 °C/decade at Miyazaki to 0.242 °C/decade at Fukuoka. The warming trends in Table 2 are statistically meaningful at the 1% level because p-values for trends at all sites are less than 0.01.
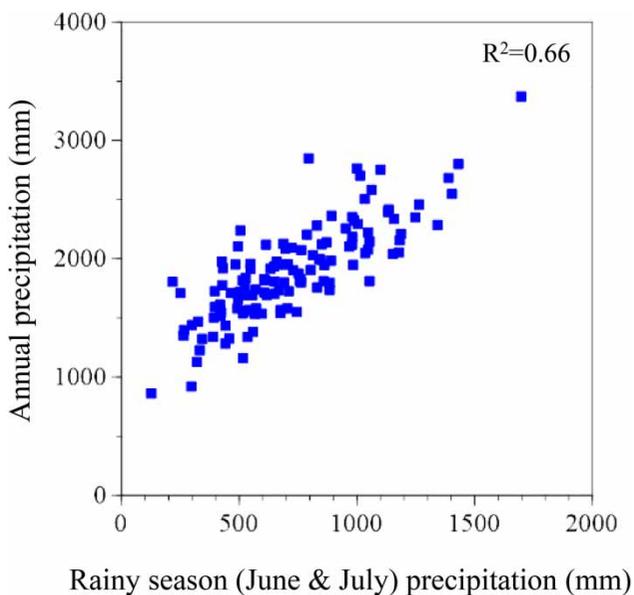
Figure 2 illustrates annual precipitation in Kumamoto from 1891 to 2018. Annual precipitation fluctuates over the period with a standard deviation of 407 mm. The linear regression line fitted to the data in Figure 2 indicates
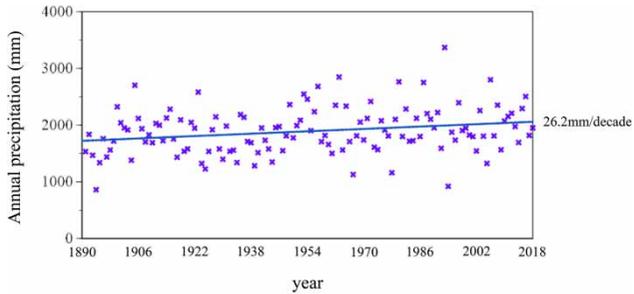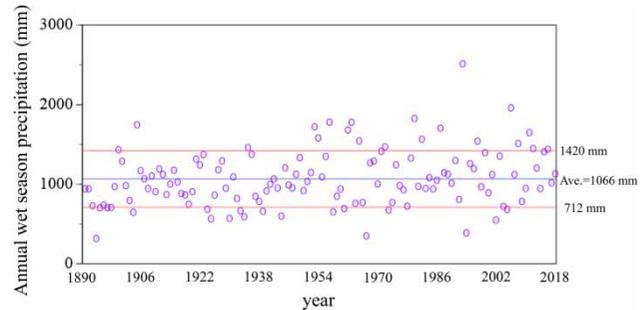
Figure 2 | Annual precipitation in Kumamoto from 1891 to 2018.

an increasing trend of 26.2 mm/decade which is 0.14% per year of the average of 1,892 mm for the period. The significances of trends were investigated by the Mann–Kendall test and are summarized in Table 3. The trend shown in Figure 2 is statistically meaningful at the 1% level, i.e. $p < 0.01$. Whereas trends in annual precipitation at the other stations are non-statistically significant, i.e. $p > 0.01$.

Rainfall during the rainy season (June and July) contributes significantly to the annual precipitation in Kumamoto. Rainy season precipitation is 12–59% of annual precipitation (average = 37%), and both have a strong correlation, i.e. $R^2 = 0.66$ as shown in Figure 3. Kyushu (Figure 1) including Kumamoto is likely to have two seasons, i.e. wet monsoon season (June–September) and dry season (October–May). Precipitation during wet and dry seasons in

Figure 3 | Comparison of annual precipitation with rainy season (June and July) precipitation in Kumamoto from 1891 to 2018.


Figure 4 | Annual wet season (June–September) precipitation in Kumamoto from 1891 to 2018.
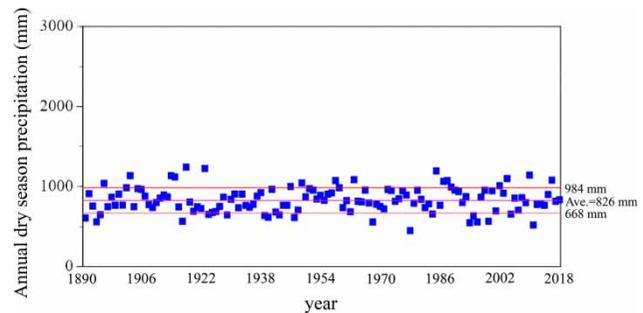
Figure 5 | Annual dry season (October–May) precipitation in Kumamoto from 1891 to 2018.

Kumamoto from 1891 to 2018 is illustrated in Figures 4 and 5, respectively. Precipitation fluctuates over the period with a standard deviation of 354 mm for the wet season and of 158 mm for the dry season. As shown in Table 3, precipitation in the wet season has a strong trend of 25.3 mm/decade, which is statistically meaningful at the 1% level, whereas the trend for the dry season is quite weak, which is non-statistically significant, and thus, can be negligible. This suggests that the increasing trend in annual precipitation in Kumamoto can be induced by an increase in precipitation in the wet season.
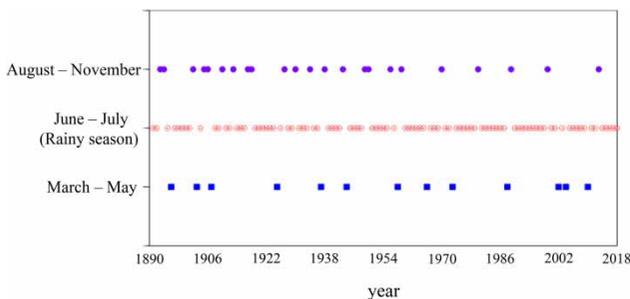
Annual maximum daily precipitation occurs in 24 h precipitation of a year and is plotted in Figure 6 from 1891 to 2018 for Kumamoto. By comparison with Figure 2, annual maximum daily precipitation has a strong increasing trend, i.e. 6.07 mm/day/decade (0.35% of the average of 172 mm/day for the period per year), which is statistically significant at the 1% level, i.e. $p < 0.01\%$ (see Table 4). Trends in annual maximum daily precipitation from 1891 to 2018 at the other stations are non-statistically significant.
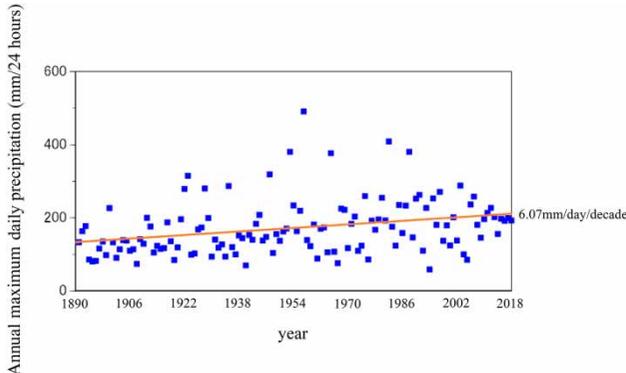
Figure 6 | Annual maximum daily precipitation in Kumamoto from 1891 to 2018.

That is similar to the trends in annual precipitation as summarized in Table 3. Change in precipitation from 1891 to 2018 at all study sites can hardly be attributed solely to air temperature rises in Table 3 because of the almost zero correlation between annual average air temperature and annual precipitation, annual maximum daily precipitation, and annual maximum hourly precipitation, i.e. $R^2 = 0.01$, 0.01, and 0.12, respectively.

As shown in Figure 7, maximum daily precipitation can be induced by either a very heavy rain in the rainy season, or a typhoon approaching Kumamoto, or even by strong precipitation occurring from March to May. Since most of the typhoons hit or approached Kumamoto from August to November, this study considers the typhoon season as August to November. As shown in Figure 7, causes of maximum daily precipitation in Kumamoto from 1891 to 2018 were typhoons 23/128 (18%), the rainy season 92/128 (72%), and others 12/128 (10%). This indicates that the rainy season has the strongest relationship to the annual maximum daily precipitation, and hence, flood risk and water resources in Kumamoto. It was also found that

typhoons have an important role in the water budget of the region, and that the interval between maximum daily precipitation events due to typhoons is becoming longer. This may be related to global warming.

Both maximum daily and hourly precipitation can be good descriptors of flood risk in the watershed. Maximum hourly precipitation in Kumamoto from 1891 to 2018 plotted in Figure 8 shows a very strong increasing trend, i.e. 2.17 mm/h/decade, which is 0.48% of the average of 45.0 mm/h for the period per year. The trend is statistically meaningful at the 1% level (see Table 5). In 50 (39%) of the 128 years, both annual maximum daily and hourly precipitation occurred on the same day. Similarly, increasing trends in Fukuoka, Nagasaki, and Kagoshima are statistically meaningful at the 1% level, whereas, in Saga, Oita, and Miyazaki, those are non-statistically significant. The trend in annual maximum hourly precipitation in Kumamoto is much stronger than that in the other cities in Kyushu. This may be due to topographical characteristics, i.e. the Kumamoto station is located in the basin, whereas the other stations are in plains. Since Kumamoto city is surrounded by mountains (Figure 1), cumulonimbus clouds develop easily when the monsoon comes from the west in the wet season.

Analysis of periodic components in the data

The square of the wavelet coefficient, i.e. $|d_k^{(j)}|^2$, is the wavelet spectrum and is illustrated in Figures 9–11 for annual precipitation, maximum daily precipitation, and maximum hourly precipitation, respectively.
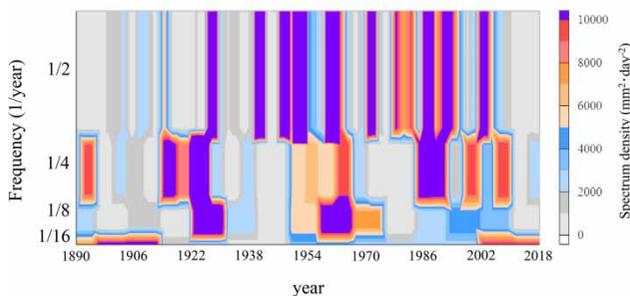
The spectrum densities of the components whose periods are 2 or 4 years become sufficiently large once

Figure 7 | Seasonal occurrence of maximum daily precipitation in Kumamoto from 1891 to 2018.
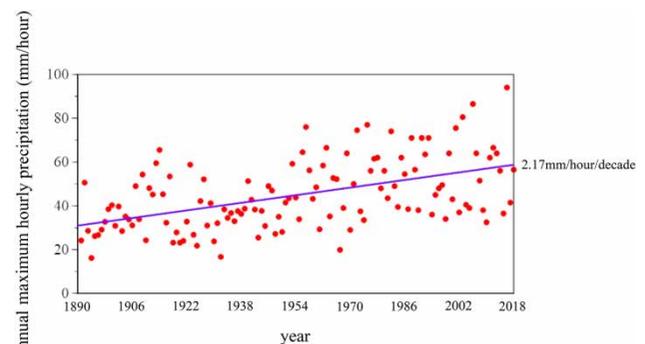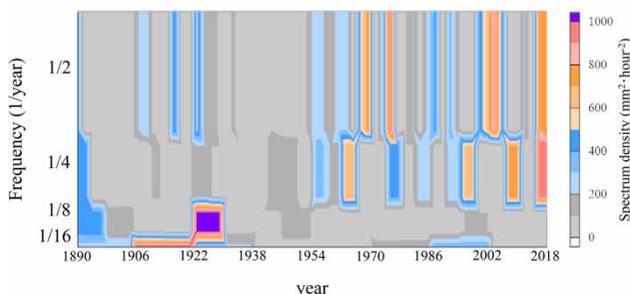

Figure 8 | Annual maximum hourly precipitation in Kumamoto from 1891 to 2018.
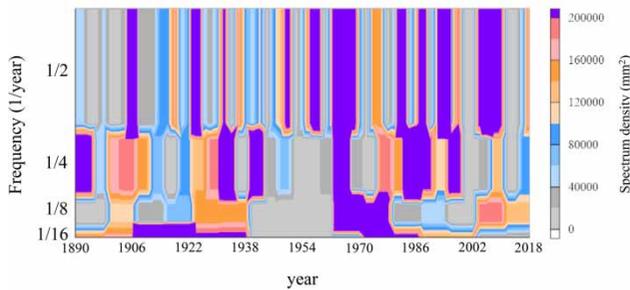
Figure 9 | Wavelet spectrum of annual precipitation in Kumamoto from 1891 to 2018.

Figure 10 | Wavelet spectrum of annual maximum daily precipitation in Kumamoto from 1891 to 2018.


Figure 11 | Wavelet spectrum of annual maximum hourly precipitation in Kumamoto from 1891 to 2018.

every several years for annual precipitation. The periodic components whose periods are 2 or 4 years may be related to the ENSO. It is known that air temperature is lower and rainfall increases during summer compared with the ordinary year due to a weakening Pacific anticyclone when El Nino is present in western Japan. One can consider that rainfall increases considerably just before, after, or when El Nino is present. Results shown in Figure 9 are consistent with Figure 2. The wavelet spectrum for annual maximum daily precipitation shows that the components

whose periods are 2 and 4 years have become significantly stronger since the 1920s. This is consistent with annual maximum daily precipitation fluctuations which have become larger since the 1920s (Figure 6), indicating that annual maximum daily precipitation has fluctuated in response to ENSO and/or typhoons since the 1920s. Annual maximum hourly precipitation has fluctuated and increased considerably after 1960 (see Figure 8) in accordance with spectrum densities whose periods are 2 or 4 years (Figure 11), which can be due to ENSO. It was reported that air temperature rises have accelerated in Japan since the 1980s (Higashino & Stefan 2020). This suggests that the effects of ENSO on annual maximum hourly precipitation become more significant as the air temperature increases. An increase in annual maximum hourly precipitation (Figure 11) may be caused by the synergistic effects of air temperature rises, ENSO, and topographical characteristics.

DISCUSSION

The sea surface temperature anomalies in the Nino 3 (Nino 3 SST index) region (4N–4S, 150 W–90 W) are an indicator of ENSO, readily available at the NOAA database (https://esrl.noaa.gov/psd/gcos_wgsp/Timeseries/Nino3/), and illustrated in Figure 12 for the 128-year period (1891–2018). Considering that ENSO is present when the sea surface temperature anomaly is higher than 1°C (El Nino), and lower than −1°C (La Nina), ENSO occurrence is summarized in Figure 13 from 1891 to 2018 by vertical straight lines of variable spacing. Annual precipitations in Kumamoto for the
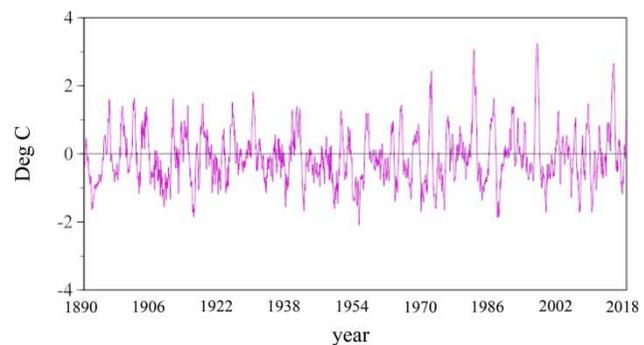

Figure 12 | Nino 3 region (4N–4S, 150 W–90 W) sea surface temperature anomalies from 1891 to 2018.
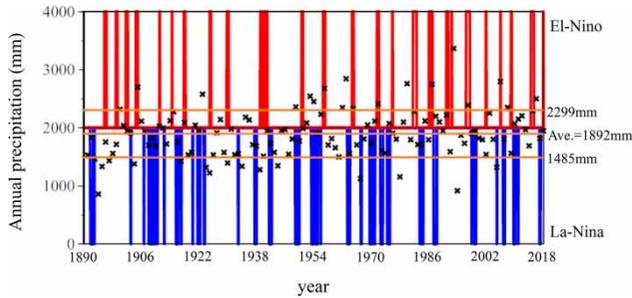
Figure 13 | Annual precipitation on Kumamoto from 1891 to 2018, and years of ENSO occurrence.

period (1891–2018) are also shown by black squares in the figure. Annual precipitation anomaly can be defined when annual precipitation is more than $\mu + \sigma = 2{,}299$ mm and less than $\mu - \sigma = 1{,}485$ mm (where μ is the average for the 128-year period $= 1{,}892$ mm, and σ is the standard deviation $= 407$ mm). As shown in the figure, precipitation in a given year may become necessarily higher or lower in phase with the ENSO, especially around the 1890s, 1900s, 1920s, 1940s, 1960–1970, and after 1990. Figure 14 illustrates the cumulative annual precipitation anomalies in response to the ENSO in Kumamoto from 1891 to 2018. It is likely that the ENSO plays an important role in annual precipitation in the periods of 1890–1900, 1920–1930, 1950–1960, 1970s, and 1990–2010.
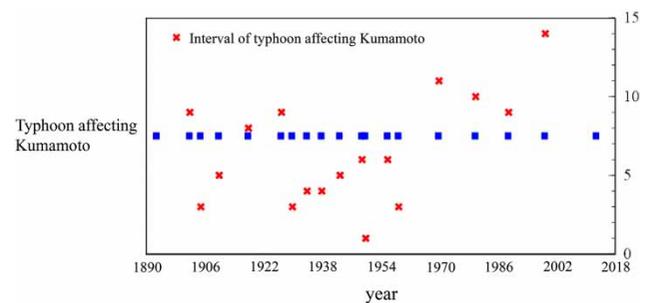
The results are consistent with the finding that the ENSO exerts a significant effect on the periodicity of precipitation in Japan. For instance, Kawamura et al. (1998) analyzed the monthly precipitation data in Fukuoka, which is about 100 km away from Kumamoto for the period from 1890 to 1999, and found that precipitation fluctuates with 4 years as one period. Also, a GCM was used to
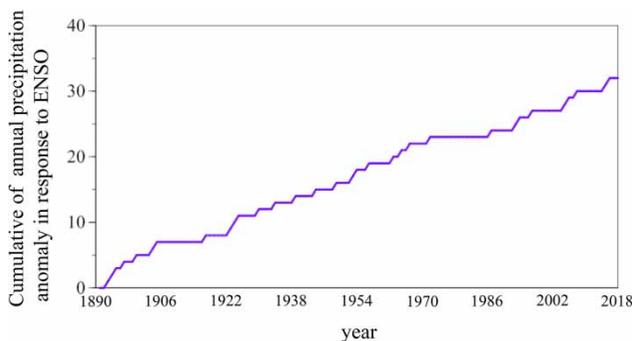
evaluate the effects of ENSO on climate in Japan (Iizuka et al. 2003). Simulated results by GCMs suggested that precipitation in Japan has a period of about 4 years, which can be related to ENSO (Kawamura et al. 2003).

The periodic components whose periods are 8 and 16 years were found to play an important role in both annual precipitation and annual maximum daily precipitation. The period of 8 or 16 years can be the frequency of big typhoons hitting or approaching Kumamoto. Figure 15 illustrates typhoons causing the maximum daily precipitation in a given year in Kumamoto from 1891 to 2018, and their interval. The interval was 8–9 years around 1900 and 1930s, which can be corresponding to the periodic component whose period is 8 years in the wavelet spectrum of annual precipitation shown in Figure 9. The interval has become longer since the 1970s, i.e. 10–14 years, which can be related to the periodic components whose periods are 8 and 16 years (Figure 9). This suggests that the effects of typhoons on precipitation in the region become more significant, and its interval gets longer as the air temperatures rise. Recent simulated results by GCMs (e.g. Sugi et al. 2002; Oouchi et al. 2006) hinted that typhoon becomes larger and the number of typhoons each year decreases as the global warming progresses. Although the air temperature has risen (Higashino & Stefan 2014), significant change in size and strength of typhoon has not been observed for the 128-year period around Japan (Japan Meteorological Agency 2018). However, it is likely that typhoons move more slowly near Kyushu (the duration of rainfall becomes longer) as the air temperature rises. The wavelet spectrum obtained in Figure 10 is consistent with Figure 6 (interval of typhoons) and significance of typhoons to precipitation in the region.

Figure 14 | Cumulative of annual precipitation anomalies in response to ENSO in Kumamoto from 1891 to 2018.

Figure 15 | Occurrence of maximum daily precipitation due to typhoon in Kumamoto and its interval from 1891 to 2018.

CONCLUSIONS

(1) Annual precipitation, annual maximum daily precipitation, and annual maximum hourly precipitation in Kumamoto, on Kyushu Island in southwestern Japan, have increased over the period from 1891 to 2018 (128 years). Trends are 26.2 mm per decade, 6.07 mm/day per decade, and 2.17 mm/h/decade, respectively. All three trends are statistically significant at the 1% level.

(2) Increasing trends in annual precipitation and annual maximum daily precipitation from 1891 to 2018 are statistically meaningful at the 1% level only in Kumamoto and are non-statistically significant in Fukuoka, Saga, Nagasaki, Miyazaki, and Kagoshima, suggesting that topographical characteristics, e.g. basin, plain, and others, play a role in increasing precipitation in the period (1891–2018).

(3) Precipitation in the rainy season (June and July) is on average 37% (range from 12 to 59%) of annual precipitation over the period from 1891 to 2018. The correlation between rainy season precipitation and annual precipitation is strong ($R^2 = 0.66$, Figure 3).

(4) Maximum daily precipitation in a year occurred at Kumamoto in the rainy (June and July) season in 92/128 (72%) of the years of observation from 1891 to 2018, in the typhoon (August to November) season in 23/128 (18%) of the years of observation and in the March to May season in 12/128 (10%) of the years of observation. This is also shown in Figure 7 and indicates that the rainy monsoon season poses the largest daily flooding risk.

(5) A wavelet analysis revealed that precipitation in Kumamoto fluctuates over the period from 1891 to 2018 with 2–4 years as one period, which may be related to ENSO. It is likely that ENSO plays an important role in annual precipitation in the periods of 1890–1900, 1920–1930, 1950–1960, 1970s, and 1990–2010, because annual precipitation in a given year becomes necessarily higher or lower in phase with the ENSO.

(6) Annual maximum hourly precipitation has fluctuated and increased significantly since 1960. The increasing trends in annual maximum hourly precipitation from 1891 to 2018 in Kumamoto were much stronger than those in the other cities. The trend is statistically significant at the 1% level. So are Fukuoka, Nagasaki, and Kagoshima, whereas Saga, Oita, and Miyazaki are not. This strong trend in Kumamoto may be attributed to the synergistic effects of air temperature rises, ENSO, and topographical characteristics.

(7) The analysis also showed that typhoons hitting or approaching Kumamoto have significantly contributed to annual precipitation and annual maximum daily precipitation, while the interval between typhoons affecting Kumamoto has been getting longer slightly since the 1970s.

REFERENCES

Alcamo, J., Doll, P., Henrichs, T., Kaspar, F., Lehner, B., Rosch, T. & Siebert, S. 2003 Development and testing of the water. GAP2 global model of water use and availability. Hydrological Science 48 (3), 317–337.

Amin, M. Z. M., Shaaban, A. J., Ercan, A., Ishida, K., Kavvas, M. L., Chen, Z. Q. & Jang, S. 2017 Future climate change impact assessment of watershed scale hydrologic processes in Peninsular Malaysia by a regional climate model coupled with a physically-based hydrology model. Science of the Total Environment 575, 12–22.

Arnell, N. W. 1999 Climate change and global water resources. Global Environmental Change 9, S31–S49.

Arora, V. K. & Boer, G. J. 2001 Effects of simulated climate change on the hydrology of major river basins. Journal of Geophysical Research 106 (D4), 3335–3348.

Chen, J., Brissette, F. P. & Leconte, R. 2011 Uncertainty of downscaling method in quantifying the impact of climate change on hydrology. Journal of Hydrology 401, 190–202.

Chow, V. T., Maidment, D. R. & Mays, L. W. 1988 Applied Hydrology. McGraw-Hill, New York.

Daubechies, I. 1992 Ten Lectures on Wavelets. Society for Industrial and Applied Mathematics, Philadelphia, PA.

Devkota, L. P. & Gyawali, D. R. 2015 Impacts of climate change on hydrological regime and water resources management of the Koshi River Basin, Nepal. Journal of Hydrology, Regional Study 4, 502–515.

Dingman, S. L. 2002 Physical Hydrology. Waveland Press, Inc., Long Grove, IL.

Farajzadeh, J. & Alizadeh, F. 2017 A hybrid linear-nonlinear approach to predict the monthly rainfall over the Urmia Lake watershed using wavelet – SARIMAX–LSSVM conjugated model. Journal of Hydroinformatics 20 (1), 246–262.

Farboudfam, N., Nourani, V. & Aminnejad, B. 2018 Wavelet-based multi station disaggregation of rainfall time series in mountainous regions. Hydrology Research 50 (2), 545–561.

Higashino, M. & Stefan, H. G. 2014 Hydro-climatic change in Japan (1906–2005): impacts of global warming and urbanization. Air, Soil and Water Research 2014 (7), 19–34.

Higashino, M. & Stefan, H. G. 2019 Variability and change of precipitation and flood discharge in a Japanese river basin. *Journal of Hydrology: Regional Studies* **21**, 68–79. doi.org/10.1016/j.ejrh.2018.12.003.

Higashino, M. & Stefan, H. G. 2020 Trends and correlations in recent air temperature and precipitation observations across Japan (1906–2005). *Theoretical and Applied Climatology*. doi:10.1007/s00704-020-03097-4.

Iizuka, S., Orito, K., Matsuura, T. & Chiba, M. 2003 Influence of cumulus convection schemes on the ENSO – like phenomena simulated in a CGCM. *Journal of the Meteorological Society of Japan* **81** (4), 805–827.

IPPC. 2014 *Climate Change 2014: Synthesis Report. Contribution of Working Groups I, II and III to the Fifth Assessment Report of the Intergovernmental Panel on Climate Change* [Core Writing Team, R.K. Pachauri and L.A. Meyer (eds.)]. IPCC, Geneva, Switzerland.

Japan Meteorological Agency. 2018 *Climate Change Monitoring Report 2017*, Tokyo, Japan.

Jemai, S., Ellouze, M. & Abida, H. 2017 Variability of precipitation in arid climates using the wavelet approach: case study of watershed of Gabes in South-East Tunisia. *Atmosphere* **8**, 178.

Kawamura, A., McKerchar, A. I., Spigel, R. H. & Jinno, K. 1998 Chaotic characteristics of the southern oscillation index time series. *Journal of Hydrology* **204**, 168–181.

Kawamura, R., Matsuura, T. & Iizuka, S. 2003 Equatorially symmetric asymmetric impacts of El Nino – Southern Oscillation on the South Asian summer monsoon system. *Journal of the Meteorological Society of Japan* **81**, 1329–1352.

Lu, Y., Qin, X. S. & Xie, Y. J. 2016 An integrated statistical and data-driven framework for supporting flood risk analysis under climate change. *Journal of Hydrology* **533**, 28–39.

Milly, P. C. D., Dunne, K. A. & Vecchia, A. V. 2005 Global pattern of trends in streamflow and water availability in a changing climate. *Nature* **438**, 347–350.

NOAA. (noaa.gov/psd/gcos – wgsp/Timeseries/Nino3/).

Nohara, D., Kitoh, A., Hosaka, M. & Oki, T. 2006 Impact of climate change on river discharge projected by multimodel ensemble. *Journal of Hydrometeorology* **7**, 1076–1089.

Oouchi, K., Yoshimura, J., Yoshimura, H., Mizuta, R., Kusunoki, S. & Noda, A. 2006 Tropical cyclone climatology in a global-warming climate as simulated in a 20 km-mesh global atmospheric model: frequency and wind intensity analyses. *Journal of the Meteorological Society of Japan* **84**, 259–276.

Palmer, M. A., Reidy Liermann, A. R., Nilsson, C., Florke, M., Alcamo, J., Lake, P. S. & Bond, N. 2008 Climate change and the world's river basins: anticipating management options. *Frontiers in the Ecology and the Environment* **6** (2), 81–89.

Partal, T. & Sezen, C. 2019 Wavelet-based analysis of global index effects in air temperature and precipitation data of the Black Sea coast. *Journal of Water and Climate Change* **10** (2), 402–418.

Rahman, A., Anik, A. M., Farhana, Z., Devnath, S. & Ahmed, Z. 2018 Pattern recognition of rainfall using wavelet transform in Bangladesh. *Open Journal of Statistics*. doi:10.4236/ojs.2018.81009.

Reshmidevi, T. V., Nagesh Kumar, D., Mehrotra, R. & Sharma, A. 2017 Estimation of the climate change impact on a catchment water balance using an ensemble of GCMs. *Journal of Hydrology* **556**, 1192–1204.

Roushangar, K., Nourani, V. & Alizadeh, F. 2018 A multiscale time–space approach to analyze and categorize the precipitation fluctuation based on the wavelet transform and information theory concept. *Hydrology Research* **49** (3), 724–743.

Santos, C. A. G., Galvao, C. d. O., Suzuki, K. & Trigo, R. M. 2001 Matsuyama City rainfall data analysis using wavelet transform. *Annual Journal of Hydraulic Engineering, JSCE* **45**, 211–216.

Sato, Y., Kojiri, T., Michihiro, Y., Suzuki, Y. & Nakakita, E. 2012 Estimates of climate change impact on river discharge in Japan based on a super-high-resolution climate model. *Terrestrial Atmos. Ocean Sci.* **23** (5), 13–24.

Schroter, D., Cramer, W., Leemans, W., Prentice, I. C., Araújo, M. B., Arnell, N. W., Bondeau, A., Bugmann, H., Carter, T. R., Gracia, C. A., Vega Leinert, A. C., Erhard, M., Ewert, F., Glendining, M., House, J. I., Kankaanpää, S., Klein, R. J. T., Lavorel, S., Lindner, M., Metzger, M. J., Meyer, J., Mitchell, T. D., Reginster, I., Rounsevell, M., Sabaté, S., Sitch, S., Smith, B., Smith, J., Smith, P., Sykes, M. T., Thonicke, K., Thuiller, W., Tuck, G., Zaehle, S. & Zierl, B. 2005 Ecosystem service supply and vulnerability to global change in Europe. *Science* **310**, 1333–1337.

Shrestha, M., Koike, T., Jaranilla-sanchez, P., Wang, L. & Wakazuki, Y. 2016 Assessment of hydrologic response to future climate change in the Tone River basin of Japan. *J. Japan. Soc. Civil Eng. Ser. B1(Hydraulic Eng.)* **72** (4), 25–30.

Sugi, M., Noda, A. & Sato, N. 2002 Influence of the global warming on tropical cyclone climatology: an experiment with the JMA global model. *Journal of the Meteorological Society of Japan* **80**, 249–272.

Taniguchi, K. 2016 Future changes in precipitation and water resources for Kanto Region in Japan after application of pseudo global warming method and dynamical downscaling. *J. Hydrol. Reg. Stud.* **8**, 287–303.

Tofiq, F. A. & Guven, A. 2015 Potential changes in inflow design flood under future climate projections for Darbandikhan Dam. *Journal of Hydrology* **528**, 45–51.

Vorosmarty, C. J., Green, P., Salisbury, J. & Lammers, R. B. 2000 Global warmer resources: vulnerability from climate change and population growth. *Science* **289**, 284–288.

Xu, Y. P., Zhang, X., Ran, Q. & Tian, Y. 2013 Impact of climate change on hydrology of upper reaches of Qiantang River Basin, East China. *Journal of Hydrology* **483**, 51–60.

Zhang, X., Xu, Y. P. & Fu, G. 2014 Uncertainties in SWAT extreme flow simulation under climate change. *Journal of Hydrology* **515**, 205–222.